

Dynamic response analysis of submerged floating tunnels by wave and seismic excitations

Jooyoung Lee^a, Chungkuk Jin^b and Moohyun Kim^{*}

Department of Ocean Engineering, Texas A&M University, 199 Spence St, College Station, Texas, USA

(Received December 29, 2016, Revised January 26, 2017, Accepted February 5, 2017)

Abstract. This paper presents the numerical simulation results for the dynamic responses of two types of submerged floating tunnels (SFT) under wave and/or seismic excitations. Time domain simulations are conducted by the commercial program OrcaFlex (OF) and in-house CHARM3D program (CP). The dynamic performances of a short/rigid/free-end SFT section with vertical and inclined mooring lines are evaluated. The SFT numerical models were validated against Oh *et al.*'s (2013) model test results under regular wave conditions. Then the numerical models were further applied to the cases of irregular waves or seismic motions. The main results presented are SFT surge/heave motions and mooring tensions. The general trends and magnitudes obtained by the two different software packages reasonably agree to each other along with experimental results. When seabed seismic motions are applied to the SFT system, the dynamic responses of SFTs are small but dynamic mooring tension can significantly be amplified. In particular, horizontal earthquakes greatly increase the dynamic tension of the inclined mooring system, while vertical earthquakes cause similar effect on vertical mooring system.

Keywords: SFT (Submerged Floating Tunnel); dynamic responses; coupled dynamics; irregular waves; earthquake; line tensions; vertical/inclined mooring

1. Introduction

Submerged floating tunnel (SFT) is considered as an alternative method for resolving the limitations of transportation caused by geographical positions. Their potential has been recognized for the past 40 years and several countries including Norway, Italy, and Japan (Di Pilato 2008) conducted feasibility studies. However, up to now, there exists no SFT and Norway just started a real project to build one. Although SFT technologies are very challenging in many aspects, it can be more cost effective and safer than under-seabed tunnels especially in seismically active regions. Engineers seeking to build SFTs are required to analyze their dynamic motions under various scenarios and reflect those analysis results for the design processes. Engineers ought to conduct thorough preliminary investigations to better understand their global performance and optimization (Brancaleoni 1989).

*Corresponding author, Professor, E-mail: m-kim3@tamu.edu

^aM.S., E-mail: jlee6590@gmail.com

^bPh.D. Student, E-mail: kenjin0519@gmail.com

Until now, many researchers have investigated the effects of random waves on SFTs. Dean (1948) investigated the interaction of waves and submerged cylindrical pipes. Maruo (1957) studied nonlinear wave forces on marine structures. Long *et al.* (2009) investigated the relationships in dynamics between the structural parameters such as buoyancy-weight ratio (BWR) and the tunnel length. Remseth *et al.* (1999) employed the finite element method to demonstrate the interactions between SFTs and wave loadings including the effects of damping and tension on SFTs. Oh *et al.*'s (2013) performed a series of model tests in regular waves for SFTs with vertical and inclined mooring systems. Cifuentes *et al.* (2015) reasonably reproduced Oh *et al.*'s (2013) experimental results by using time-domain simulation programs.

In addition to the hydrodynamic loads, such as waves and currents, other natural disasters can also influence on the global performance of SFTs. Marine earthquake is one of the issues for the safety of SFTs. Since the significant earthquake event at Kobe in 1995, researchers have studied the influence of earthquakes on SFT's safety and performance through both analysis and numerical methods.

Brancaleoni (1989) investigated the dynamic responses of short-span and long-span SFTs under seismic conditions. Fogazzi and Perotti (2000) used a numerical procedure to analyze the dynamic response of a seabed-anchored SFT under extreme seismic excitations. The non-stationary responses of suspension bridges with multiple-support SFT under earthquake excitations were investigated by Hyun *et al.* (1992). Their results showed that the effect of horizontal seismic motion was more significant than vertical motion. Chen and Huang (2010) numerically studied the dynamic characteristics of a SFT by seismic wave passage effect. Di Pilato *et al.* (2008) investigated a SFT as a multi-supported structure associated with seismic waves. Lee *et al.* (2016) performed a numerical study on the effects of earthquake-induced acoustic waves due to fluid compressibility on pressures over structures with varying seawater depth and tunnel location. Those seawater compressibility effects are not important for the global dynamics of SFT, so not considered in the present study.

In this research, we conducted numerical simulations of SFTs with vertical and inclined mooring system under sea waves and/or seismic excitations. The time-domain simulations are carried out using the commercial program OrcaFlex (OF) and in-house program CHARM3D (CP) that has been developed by the 3rd author's research group during the past two decades (e.g., Kang and Kim 2014, Yang and Kim 2010). Both regular and irregular water waves and seismic motions are inputted. In the earthquake cases, the transmissibility of the ground motions through two types of mooring lines to the SFT responses is investigated. In this regard, real seismic displacement data with varying amplitudes obtained from California and Hawaii earthquakes are employed as input seismic excitations.

2. Modeling of the SFT and mooring configurations

The basic configurations with vertical and inclined mooring line configurations are shown in Fig. 1. The dimension of the SFT is a length of 98 m, a diameter of 23 m, and a wall thickness of 1 m. The SFT with vertical mooring lines is referred to as SFT-VM and the SFT with inclined mooring lines is called as SFT-IM. The mooring lines of SFT-VM and SFT-IM are 90 degrees and 60 degrees to the ground, respectively. All mooring lines are of diameter 0.12 m with density 8000 kg/m³ and elastic modulus 197 GPa. The BWR is 2.6. The water depth is 80 m and the submerged depth is 41.5 m. The SFTs were designed by Oh *et al.* (2013), who also conducted experiments

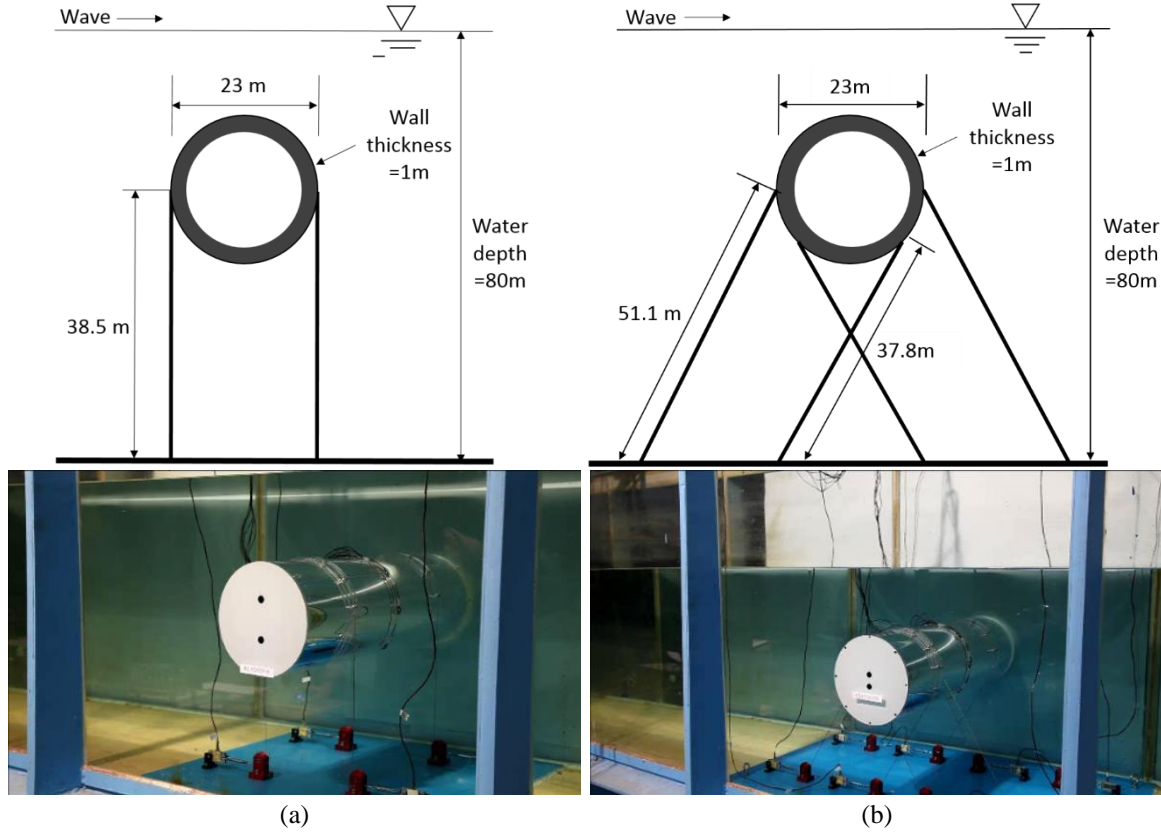


Fig. 1 Basic mooring configurations of SFT (a) SFT with vertical mooring (SFT-VM), and (b) SFT with inclined mooring (SFT-IM); The pictures are taken from Oh *et al.*'s (2013) experimental set up

with the 1:100-scale model in regular wave conditions.

3. Equation of motion under seismic excitation and numerical simulation description

The dynamics of moored structures under wave/seismic excitations are solved in time domain by time marching simulations. The governing equation for the 3DOF motion (surge, heave, and pitch) is given by

$$(M + M_{Add}(\infty))\ddot{x}(t) + (K_{hydro})x(t) = F_{wave} + F_{drag} + F_{mooring} \quad (1)$$

where M is mass, M_{Add} is added mass, K_{hydro} is hydrostatic restoring coefficient, F_{wave} is wave exciting force, and $F_{mooring}$ is mooring-induced force. \ddot{x} and x are acceleration and displacement of the structure, respectively. Morison equation is generally used to calculate the wave loads on slender cylindrical structures. This equation is expressed in terms of the linear inertia and quadratic drag loads. In case of earthquake simulations, the acoustic-pressure induced force is neglected in the right hand-side of (1) and only the movements of anchor points are inputted. The total wave load per unit length for a moving structure is represented as follows

$$F = C_M \rho \frac{\pi D^2}{4} \ddot{\eta} - C_A \rho \frac{\pi D^2}{4} \ddot{x} + \frac{1}{2} \rho C_D D |\dot{\eta} - \dot{x}| (\dot{\eta} - \dot{x}) \quad (2)$$

where ρ is the water density, C_A is the added mass coefficient, $C_M (=1+C_A)$ is the inertia coefficient, C_D is the drag coefficient, D is the diameter of the cylindrical structure, $\dot{\eta}$ and $\ddot{\eta}$ are wave-induced velocity and acceleration, and \dot{x} and \ddot{x} are the velocity and acceleration of the structure. The second term of (2) is equivalent to the added mass term of (1) in the left-hand side. F_{wave} consists of the first and third terms of (2). In this study, the wave loads on the SFTs are computed by means of the above Morison equation with linear wave kinematics. On the other hand, the simulation of the seismic excitation is conducted by moving the anchor points of the mooring lines at each time step as prescribed ground motions.

In the simulations, the inertia coefficient, C_M , is 2 ($C_A=1$) for both OF and CP because the SFTs are deeply submerged circular cylinders. In the case of the drag coefficient, C_D , while CP uses a constant drag coefficient of 1.2, the DeCew (2010) formulation is used in OF. In the DeCew (2010) formulation, C_D is a function of Reynolds number as follows

$$C_D = \begin{cases} \frac{8\pi}{Re} (1 - 0.87s^{-2}), & 0 < Re < 1 \\ 1.45 + 8.55Re^{-0.9}, & 1 < Re \leq 30 \\ 1.1 + 4Re^{-0.5}, & 30 < Re \leq 2.33 \times 10^5 \\ -3.41 \times 10^{-6} (Re - 5.78 \times 10^5), & 2.33 \times 10^5 < Re \leq 4.92 \times 10^5 \\ 0.401(1 - e^{-Re/5.99 \times 10^5}), & 4.92 \times 10^5 < Re \leq 10^7 \end{cases} \quad (3)$$

$$s = -0.077215655 + \ln(8/Re)$$

In case of OF, the Wheeler stretching method (Wheeler 1969) was used along with Airy's linear wave theory for the wave induced water-particle velocity and acceleration, while CP used the original Airy wave theory. For example, the horizontal particle velocity in Airy wave theory is

$$u(x, z, t) = \omega \eta_a \frac{\cosh(k(z+h))}{\sinh(kh)} \sin(\omega t - kx) \quad (4)$$

where ω is angular frequency, k is wave number, η_a is wave amplitude, and h is water depth. The term, $\cosh(k(z+h))/\sinh(kh)$, leads to exponential decay of velocity with z . In Wheeler stretching method, better estimation of velocity and acceleration may be made by replacing the vertical coordinate, z , with z' as follows

$$z'(x, t) = \frac{h(h+z)}{h+\eta(x, t)} - h \quad (5)$$

where η is wave elevation. In both computer programs, the Morison forces are evaluated at SFT's instantaneous positions at each time step. For mooring line analyses, OF used massless springs, which represent axial, bending, and torsional behaviors. The springs are connected to nodes where mass, weight, buoyancy, and other properties are lumped (Orcina 2015). Mooring line analysis of CP is based on the high-order finite element (FE) method using extensible slender-rod elements without twisting (Garrett 1982). The governing equation was formulated along the generalized coordinate system (Garrett 1982). The line dynamics is fully coupled with floater motions by solving the whole system in a combined matrix. The line dynamics includes the effect of gravity force, hydrodynamic loads, and ground boundary conditions.

4. Wave and seismic conditions

As described above, SFT experiments in regular wave conditions were performed by Oh *et al.* (2013). Cifuentes *et al.* (2015) carried out numerical simulations to compare with their experimental results. The experiment results for regular waves are also utilized in this paper to validate our numerical model. These regular-wave conditions are given in Table 1.

After validating the numerical model, we next considered the SFT dynamics simulation in more realistic irregular waves. JONSWAP wave spectrum with enhancement parameter γ of 3.3 is used for irregular-wave simulations. In the CP case, the irregular waves are generated by superposing 100 wave components with randomly perturbed interval to avoid signal repetition. Table 2 gives

Table 1 Regular wave conditions

Wave Period (s)	Wave Height (m)	Wave Steepness
6.5	0.85	0.013
	1.75	0.027
	2.65	0.040
	3.50	0.053
8.0	1.30	0.013
	2.70	0.027
	4.00	0.040
	5.30	0.053
10.0	2.00	0.013
	4.10	0.027
	6.20	0.040
	8.20	0.053
13.0	3.20	0.013
	6.50	0.027
	9.80	0.040
	13.00	0.053

Table 2 Irregular wave conditions

Case #	Significant Wave height (m)	Peak period (s)
1	0.09	2.0
2	0.67	4.8
3	1.40	6.5
4	2.44	8.1
5	3.66	9.7
6	5.49	11.3
7	9.14	13.6
8	15.24	17.0

Table 3 Characteristics of earthquake conditions

Earthquake	Magnitude (Richter scale)	Horizontal Peak motion (cm)	Vertical Peak motion (cm)
Green Valley, California	3.9	-0.03	-0.0107
Honomu, Hawaii	4.9	0.06	-0.00347
Offshore Northern, California	5.4	0.16	0.0743
WNW of Ferndale, California	6.8	2.20	-1.7

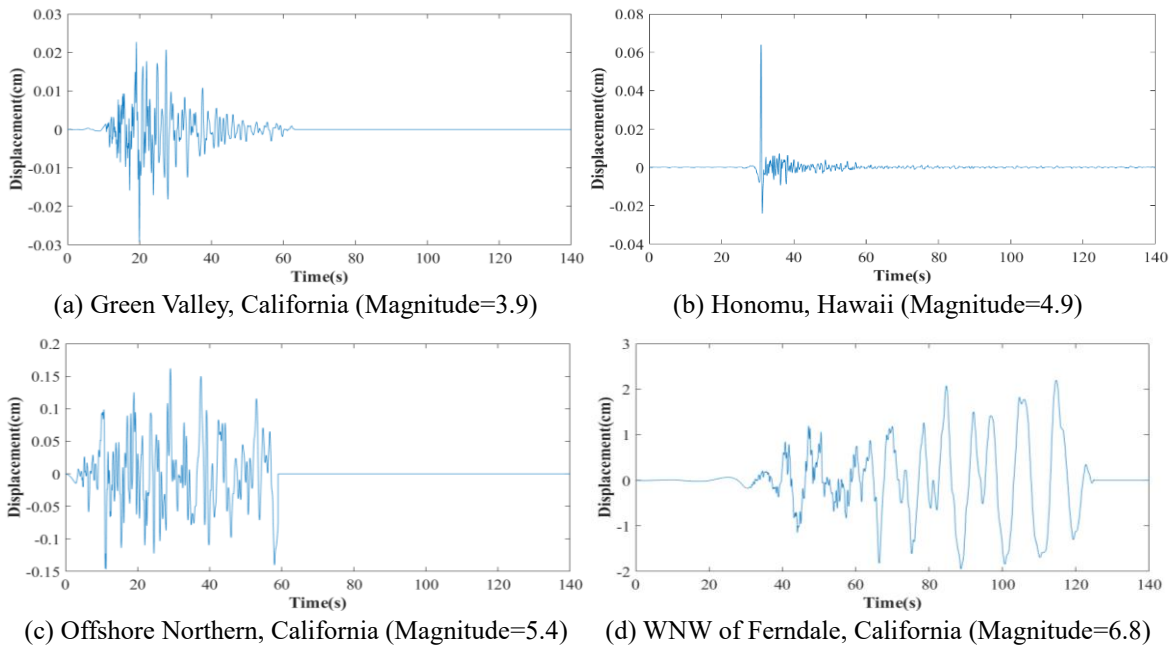


Fig. 2 Real horizontal seismic motions for 140 sec

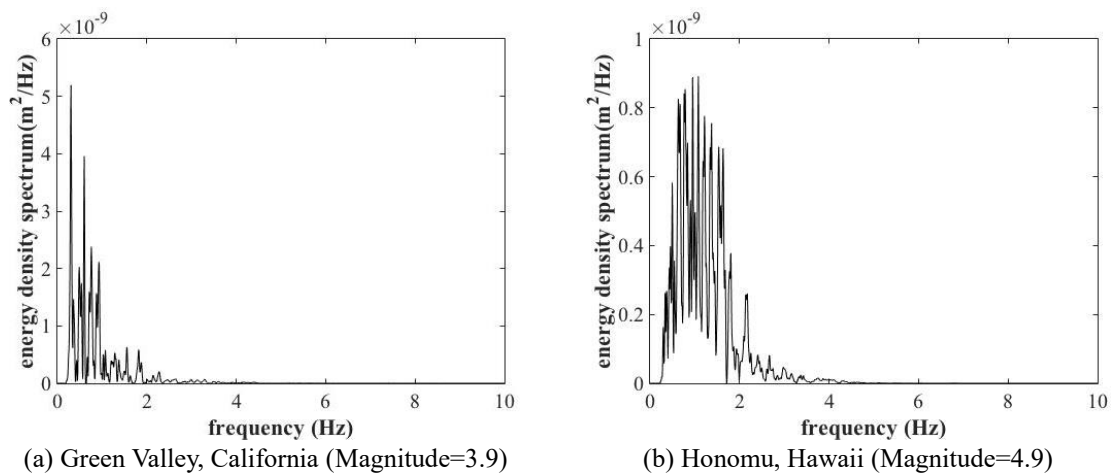
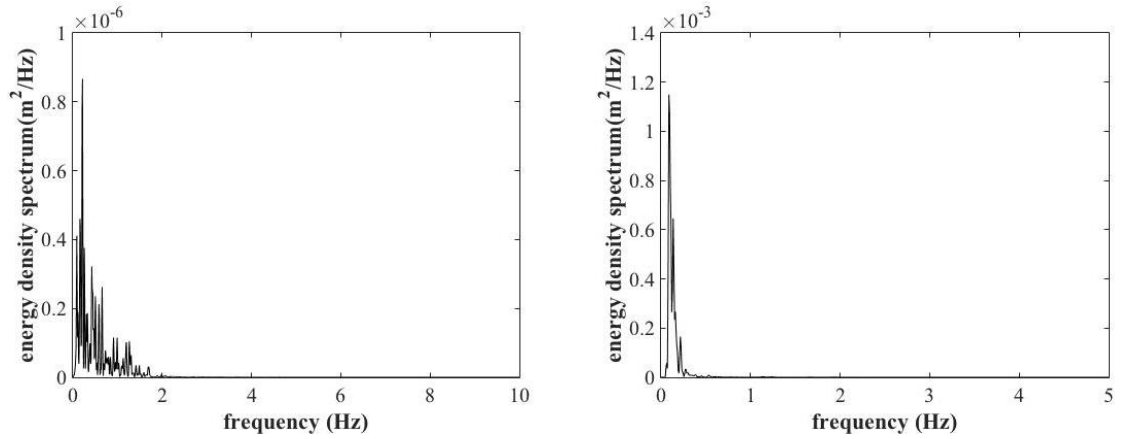
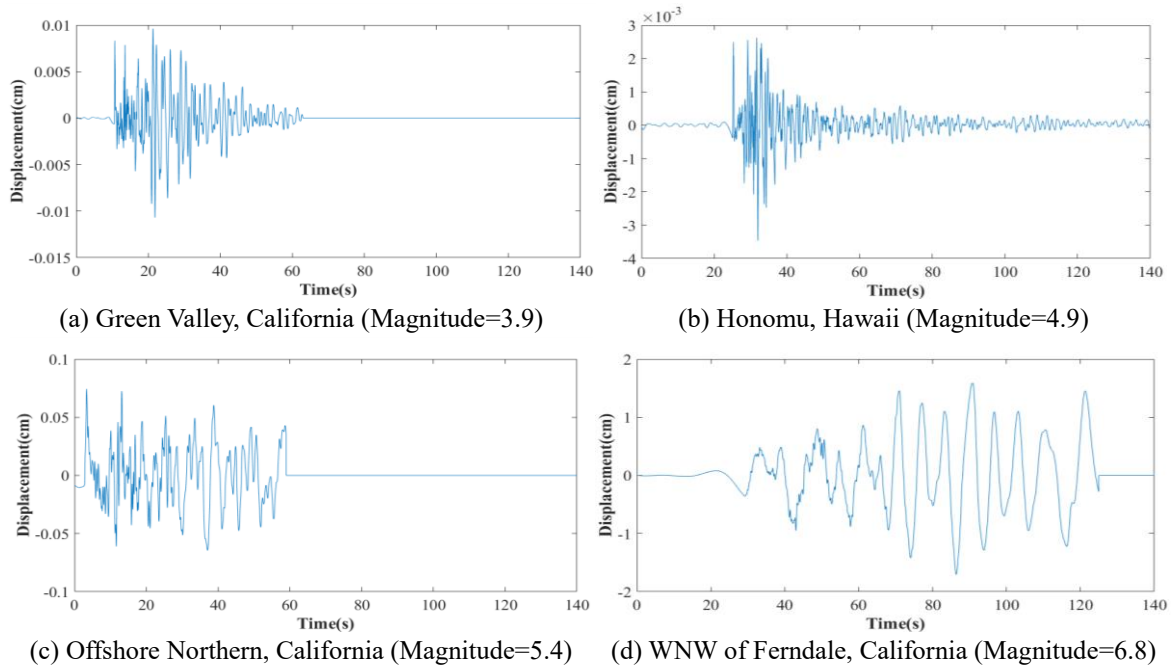


Fig. 3 Energy density spectrum of real horizontal seismic motions



(c) Offshore Northern, California (Magnitude=5.4) (d) WNW of Ferndale, California (Magnitude=6.8)
Fig. 3 Continued



(c) Offshore Northern, California (Magnitude=5.4) (d) WNW of Ferndale, California (Magnitude=6.8)

Fig. 4 Real vertical seismic motions for 140 sec

irregular wave conditions. Eight wave conditions are selected based on significant wave height and peak period, and 3-hour simulations are performed for each wave case. To have the same irregular-wave condition in OF runs as the CP case, the wave elevation time series generated from CP is directly used in OF simulations.

Next, the dynamic responses of SFTs due to submarine earthquakes are also investigated. To check the robustness of SFT mooring system under seismic conditions, both harmonic and random seismic motions in horizontal and vertical directions are applied, which have frequencies of 0.5

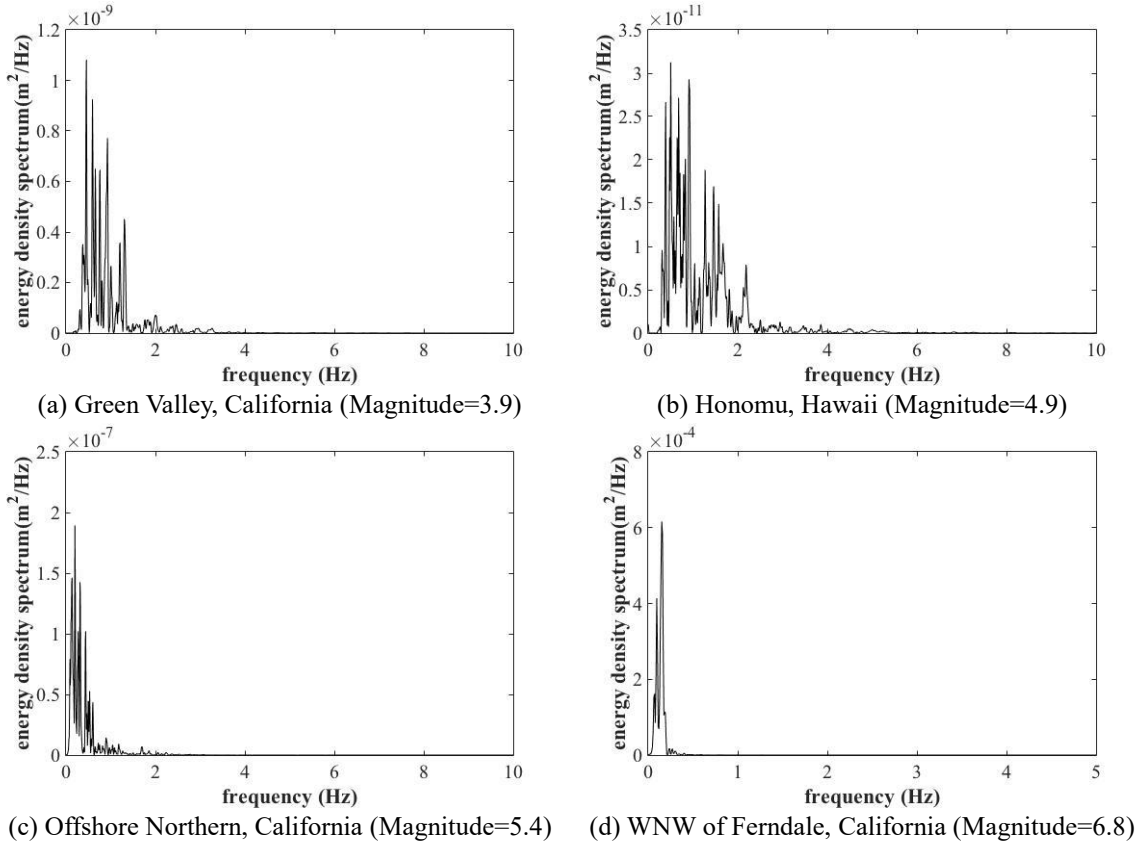


Fig. 5 Energy density spectrum of real vertical seismic motions

Hz, 0.75 Hz, 1.0 Hz, and 1.25 Hz, and amplitudes of 0.1 m, 0.2 m, 0.05 m and 0.01 m. In addition, four real seismic motions in horizontal and vertical directions are employed to examine the corresponding global performance of SFTs. The characteristics of the real seismic motions applied are given in Table 3. The time histories and corresponding spectra of the ground motions are illustrated in Figs 2-5.

4. Simulation result

4.1 Regular wave - Validation of numerical models against experimental results

To validate the numerical models by CP and OF, the numerical simulation results under regular wave conditions are first compared with the experimental results of Oh *et al.* (2013).

Fig. 6 shows the results of SFT-VM and SFT-IM side by side. In cases of SFT-VM, the numerical simulation results reasonably reproduced the general trend of surge/heave responses and mooring-line tensions compared with the measured data. In cases of SFT-IM, the corresponding experimental data were not available. However, the two numerical simulation results, OF and CP, agree reasonably to each other. Their discrepancies for the extreme wave conditions can be

attributed to the differences in drag coefficients and wave kinematics formulas, as explained in the previous section. For further validation of the SFT-IM design, the numerical simulations for the case BWR=3.4 were conducted and compared with available experimental data under the same conditions. Fig. 7 shows the tension comparison, in which the general trend of numerical simulations agrees reasonably with experiment data.

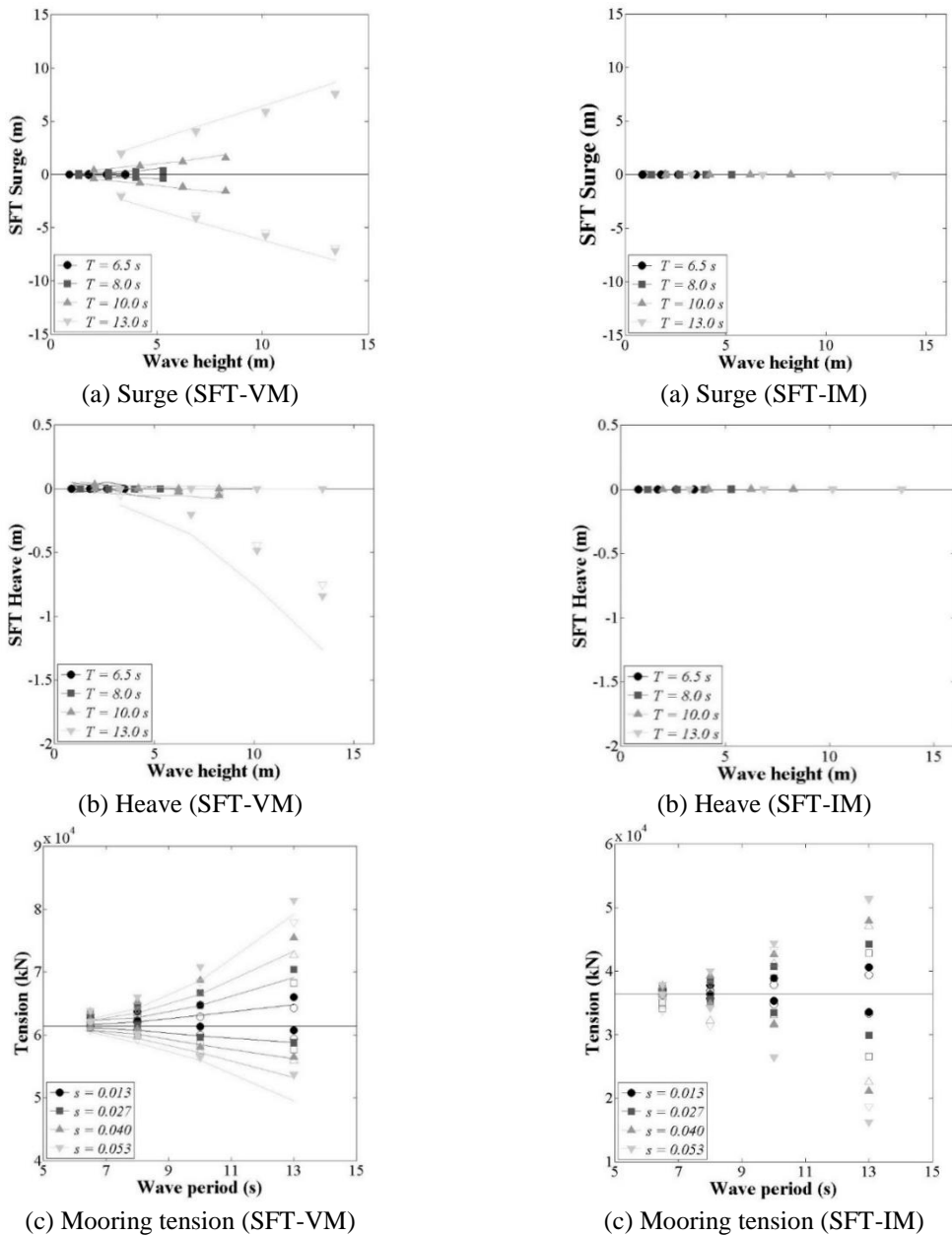


Fig. 6 Comparison of CP and OF results to the experiments in regular wave conditions. (solid lines represent experiments, open marks represent OF and solid marks indicate CP)

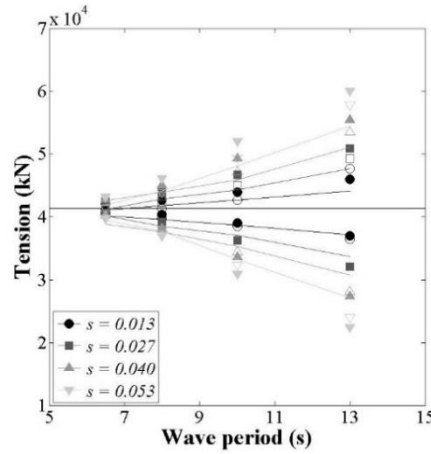


Fig. 7 Comparison of mooring line tension (at fairlead) of SFT-IM with the experiments in regular wave conditions. (solid lines represent experiments, open marks represent OF and solid marks indicate CP)

In case of SFT-VM, the downward heave motion can be large in long waves with large amplitudes due to slackness and set-down effect. The large downward motion can potentially cause compressional loads and the risk of buckling. However, the inclined mooring system can prevent the problem. The vertical mooring system also has weak stiffness in surge, so its surge motions in long and large waves are large. However, inclined mooring system significantly reduced the surge and heave motions even for the worst (largest and longest) wave condition. The differences between numerical and experimental results can be attributed to nonlinear and diffraction/radiation effects and more subtle viscous effects, which can further be tuned by adjusting inertia and drag coefficients and using nonlinear wave kinematics.

In the SFT-VM and SFT-IM, 4 and 8 mooring lines are used respectively. Therefore, the maximum tension of SFT-IM is about 25% smaller than that of SFT-VM. At any rate, SFT-IM is much better in overall dynamic performance but may be more expensive compared to SFT-VM. Since the results of the numerical simulations by means of OF and CP agreed reasonably with those of the experiments, it is subsequently applied in the next sections to more realistic irregular-wave or marine-earthquake environments.

4.2 Result of irregular-wave condition

SFTs in irregular waves are examined via numerical simulations by means of OF and CP. As described above, irregular wave conditions (see Table 2) are assumed through a JONSWAP spectrum with a γ of 3.3. The Morison equation may not be very accurate in short-wave regime but the particle kinematics of short waves decay fast with depth, so wave effects become small and unimportant anyway near the SFT position.

The surge/heave responses and mooring tensions under the irregular wave conditions using OF are summarized in Table 4. Figs. 8 and 9 show the maximum surge motions and mooring tension in the irregular wave conditions by OF and CP. The general trend of surge, heave, and mooring tensions in irregular-wave simulations are similar to those in the regular-wave ones. Moreover, the

Table 4 Maximum and minimum values of the responses and tensions in irregular waves using OF

Case#	Significant Wave height (m)	Peak period (s)	Surge (m)		Heave (m)		Tension (kN)	
			Min.	Max.	Min.	Max.	Min.	Max.
1	0.09	2.0	0.000	0.000	0.001	0.000	63925	63925
2	0.67	4.8	-0.006	0.006	0.001	0.000	63867	63989
3	1.40	6.5	-0.082	0.092	0.001	0.000	63392	64529
4	2.44	8.1	-0.454	0.464	-0.001	0.000	61870	66181
5	3.66	9.7	-1.401	1.528	-0.029	0.002	59780	69391
6	5.49	11.3	-4.075	4.658	-0.282	0.003	58297	73718
7	9.14	13.6	-12.559	15.070	-3.073	0.005	48396	89513
8	15.24	17.0	-21.626	27.950	-9.893	0.012	35514	126075

(a) SFT with vertical mooring line

Case#	Significant Wave height (m)	Peak period (s)	Surge (m)		Heave (m)		Tension (kN)	
			Min.	Max.	Min.	Max.	Min.	Max.
1	0.09	2.0	0.000	0.000	0.000	0.000	36248	36248
2	0.67	4.8	0.000	0.000	0.000	0.000	36169	36329
3	1.40	6.5	0.000	0.000	0.000	0.000	35497	37026
4	2.44	8.1	-0.001	0.001	0.000	0.000	33344	39344
5	3.66	9.7	-0.002	0.002	-0.001	0.001	29881	43485
6	5.49	11.3	-0.003	0.003	-0.001	0.001	25875	47554
7	9.14	13.6	-0.006	0.006	-0.002	0.002	18376	56196
8	15.24	17.0	-0.012	0.010	-0.003	0.003	4999	77628

(b) SFT with inclined mooring line

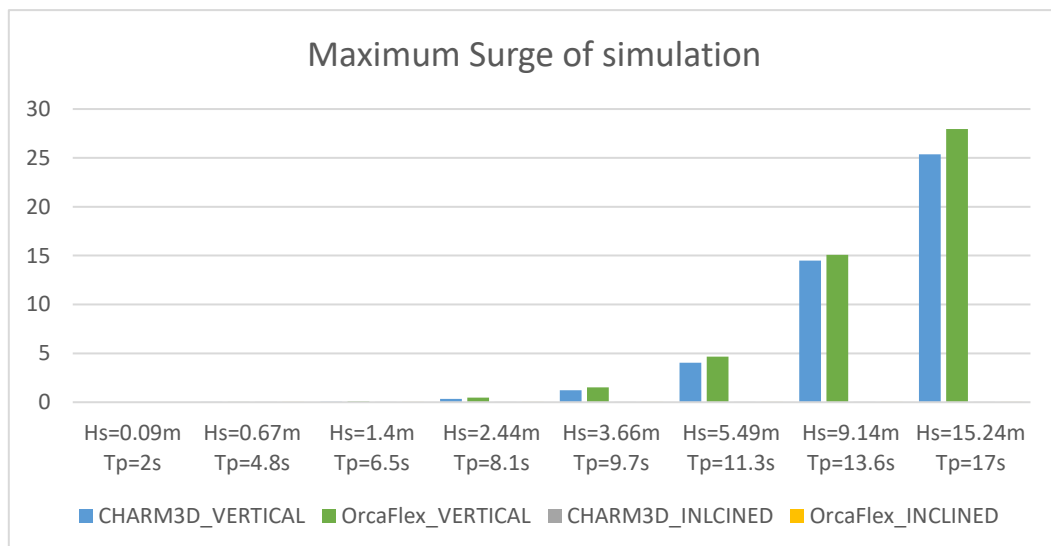


Fig. 8 Numerical results for maximum surges for SFT-VM and IM from CP and OF in terms of significant wave height and peak period

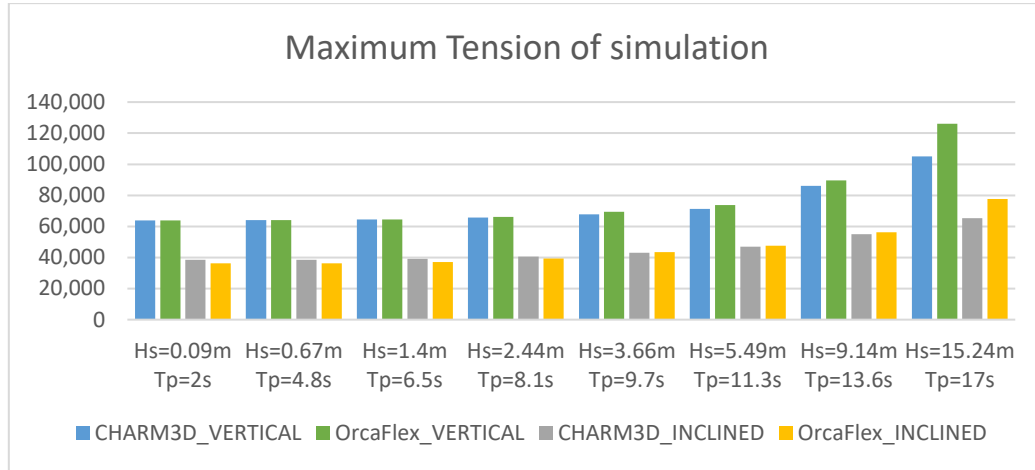


Fig. 9 Numerical results for maximum tension for SFT-VM and IM from CP and OF in terms of significant wave height and peak period

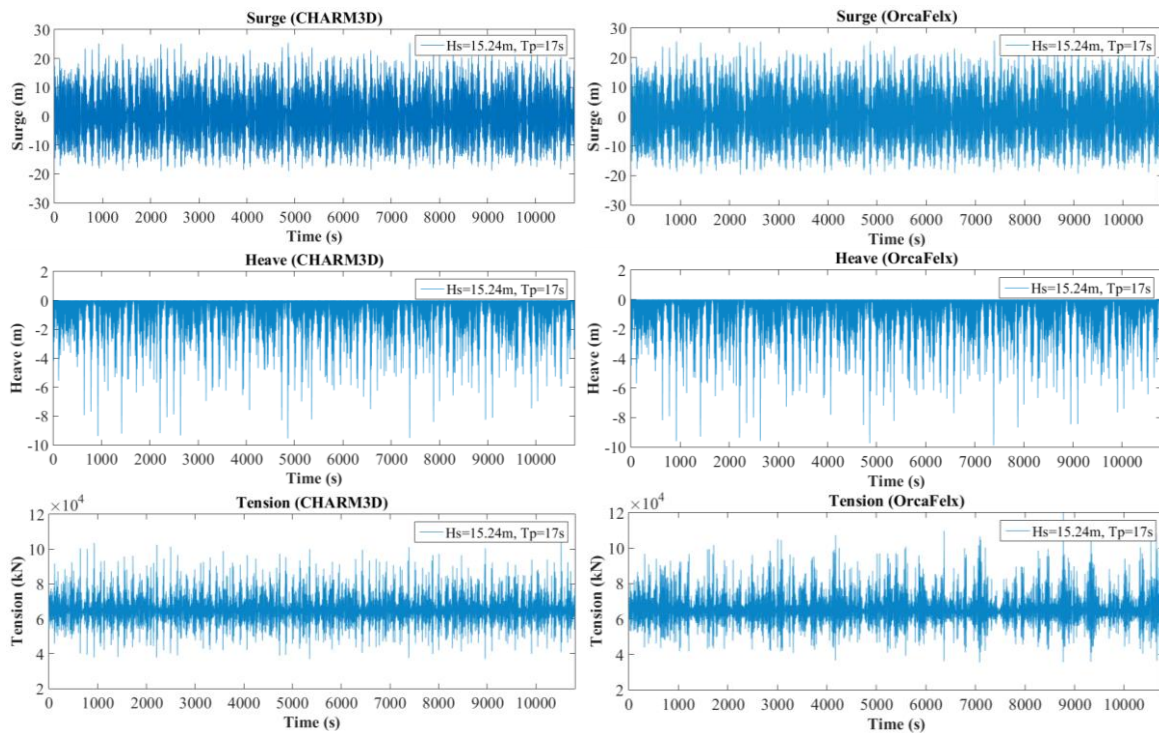


Fig. 10 Numerical results for the (a) surge, and (b) heave (c) tension of SFT-VM from OF, and CP in irregular waves at significant wave height 15.24 m and peak period of 17 s

results obtained from OF (see Figs. 8 and 9) well coincide with those from CP except for Case 8 (significant wave height of 15.24 m and peak wave period of 17 s). However, the difference is less than 10%. Since the same input is used for incident irregular waves, the difference is most

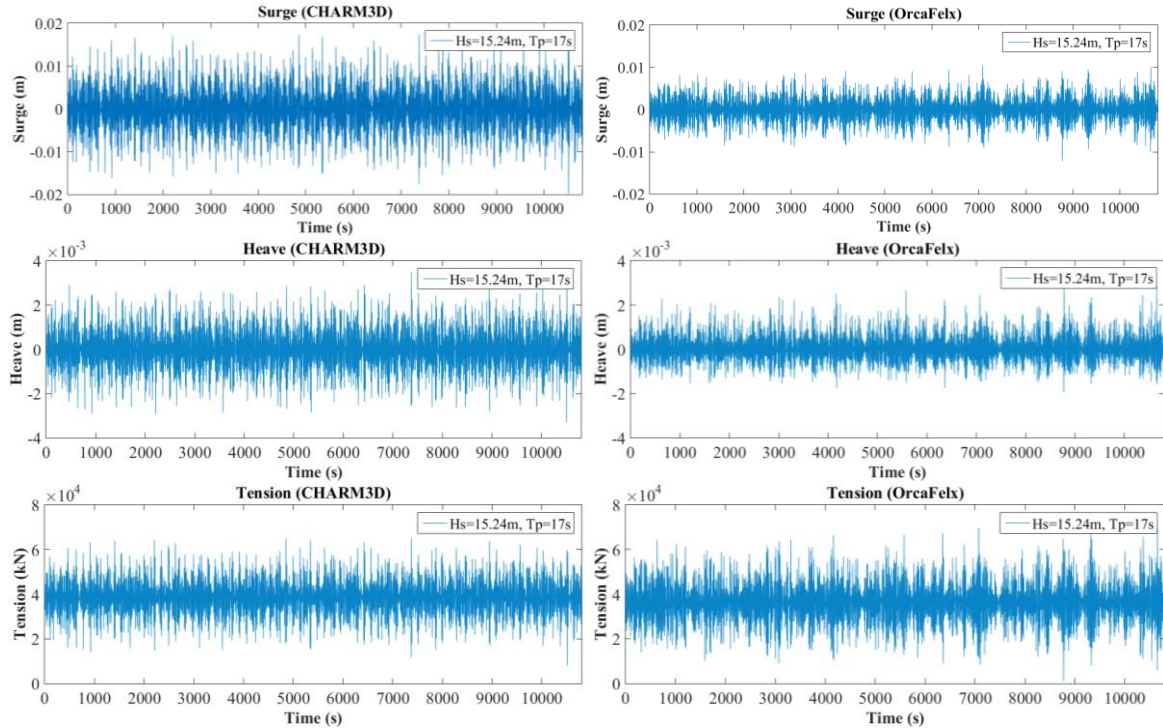


Fig. 11 Numerical results for the (a) surge, and (b) heave (c) tension of SFT-IM from OF, and CP in irregular waves at significant wave height 15.24 m and peak period of 17 s

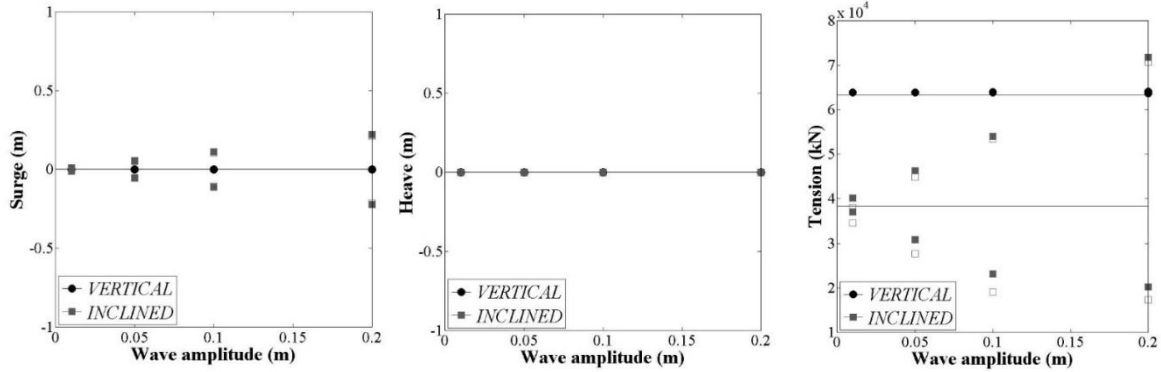
likely caused by different drag coefficients (application of DeCew formula in OF) and the usage of Wheeler stretching method in OF. As in the regular-wave cases, the surge and heave motions of SFT-VM are critically larger than those of SFT-IM in harsher wave conditions. For example, as shown in Figs. 10 and 11, the maximum surge motion of SFT-VM is more than 25 m for Case 8, while that of SFT-IM is only 0.01 m. In addition, the minimum heave motion of SFT-VM is -9.9 m for Case 8, while that of SFT-IM is only -0.003 m.

Fig. 9 shows the mooring tensions for SFT-VM and SFT-IM. Generally, both mean and dynamic tensions of SFT-VM are significantly larger than those of SFT-IM (the maximum difference between these two types of SFT is approximately 38%). Considering that 8 lines were used in SFT-IM compared to 4 lines of SFT-VM, the smaller maximum tension on each line of SFT-IM can somewhat be expected. The overall performance of SFT-IM in restricting SFT surge and heave responses is much better than that of SFT-VM. The large surge and heave responses of SFT-VM in harsh wave conditions are actually significantly exaggerated since both ends of the model SFT are free. In reality, it is a small portion of long SFT which is to be fixed at both ends.

4.3 Result of seismic condition

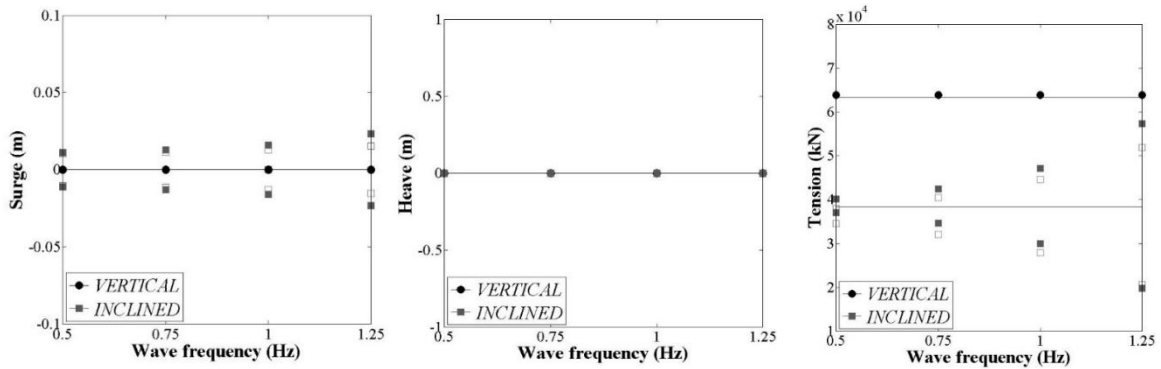
4.3.1 Effects of harmonic seismic motions

In this section, we consider the same SFT-VM and SFT-IM models under seismic excitations instead of waves. The numerical models are modified to simulate the earthquake cases with



(a) Surge (Constant Frequency) (b) Heave (Constant Frequency) (c) Mooring tension (Constant Frequency)

Fig. 12 Earthquake-induced surge, heave, and mooring tension (at fairlead) of SFT-VM and SFT-IM as functions of amplitude at a frequency of 0.5 Hz. (open marks represent OF and solid marks indicate CP.)



(a) Surge (Constant Amplitude) (b) Heave (Constant Amplitude) (c) Mooring tension (Constant Amplitude)

Fig. 13 Earthquake-induced surge, heave, and mooring tension (at fairlead) of SFT-VM and SFT-IM as functions of frequency at an amplitude of 0.01 m. (open marks represent OF and solid marks indicate CP.)

specified horizontal and vertical ground motions. It is assumed that the seabed is flat and all the anchored points are excited by the same ground motions. Then, the global performances of the two types of SFTs are simulated, checked, and assessed. First, harmonic ground motions are considered. The frequencies of the harmonic seismic motions are 0.5 Hz, 0.75 Hz, 1.0 Hz, and 1.25 Hz, and horizontal ground-motion amplitudes are 0.2 m, 0.1 m, 0.05 m, and 0.01 m. The selected frequencies and amplitudes are the representative values of medium to small scale earthquakes. These sinusoidal seismic motions are applied at the anchor points.

Fig. 12 shows surge, heave, and mooring tension of SFT-VM and SFT-IM as functions of amplitude at a frequency of 0.5 Hz. Fig. 13 shows surge, heave, and mooring tension of SFT-VM and SFT-IM as functions of frequency at a given amplitude of 0.01 m. In both cases, the results obtained from OF coincide well with those from CP. While the surge magnitude in SFT-IM is

generally similar to the applied seismic motion, that in SFT-VM is much smaller than the applied seismic motion. It is because the vertical mooring does not directly pull the surge motion. The surge motion of SFT-VM is 0.5% to 1.2% of the applied seismic motions. The heave motions of both mooring system are negligible under this horizontal ground motion. In addition, even though the mooring pretension of SFT-VM is much larger than SFT-IM, the maximum mooring tension of SFT-IM can significantly increase with ground-motion amplitude. When the amplitude is 0.2 m, the maximum mooring tension of SFT-IM exceeds that of SFT-VM. The mooring tension of SFT-VM does not increase considerably with the increase in horizontal ground-motion amplitude. In Fig.13, the surge and mooring tension also increase with the increase of frequency in the case of SFT-IM. In general, the surge of SFT-VM is much larger than that of SFT-IM with the applied horizontal ground motions.

4.3.2 Effects of random seismic motions

The real seismic ground excitations in horizontal and vertical directions are applied to the SFT-VM and SFT-IM. Fig. 14 shows the maximum surge, heave, and mooring tension as functions of earthquake magnitude after applying the random ground excitations in the horizontal direction. In general, the maximum surge and heave motions of both SFTs increase with earthquake magnitude. The maximum surge motion of SFT-VM is less than that of SFT-IM, which has the same tendency as in the harmonic seismic motion case. The maximum heave motions of SFT-VM are very small and similar to those of SFT-IM. The maximum tensions of SFT-VM remain almost the same regardless of horizontal earthquake magnitude because the vertical mooring cannot directly transfer the dynamics of horizontal ground motions. On the other hand, the maximum mooring tensions of SFT-IM increase significantly with the increase in horizontal earthquake magnitude because the inclined mooring lines have to more directly pull the SFT. When the earthquake magnitude is 6.8, the maximum mooring tension of SFT-IM exceeds that of SFT-VM. In particular, the maximum tension of SFT-IM is as significant as the extreme wave condition. As given in Table 4, the maximum tension of SFT-IM in case 8 (significant wave height of 15.24 m and peak period of 17 s) in the irregular wave condition is similar to that of the real seismic excitation of magnitude of 6.8. In conclusion, the seismic excitations do not cause serious SFT motions but the resulting dynamic mooring tensions can be serious. Seismic motions greater than magnitude of 6.8 occur more often than not in seismically active zones. In such situations, the mooring line design has to be carefully checked for proving its structural robustness. At any rate, SFTs are to be much less vulnerable to marine earthquakes than under-seabed tunnels.

Figs. 15 and 16 show the time series of surge, heave, mooring tension, and the amplitude spectrum for surge motion of SFT-VM (Fig. 15) and SFT-IM (Fig. 16) with horizontal earthquake of magnitude 6.8. The results by OF well coincide with those of CP for both mooring cases. The dynamic mooring tension of SFT-VM is very small, while that of SFT-IM is very significant, as was discussed in the above. It is found that the maximum tension occurs at the fairlead positions even for the earthquake cases as in the wave cases. The SFT-VM is softer than SFT-IM in surge direction, so the surge frequencies of SFT-VM are lower than those of SFT-IM. The present earthquake simulations are for the SFT with free end conditions. If both ends are fixed with relatively short span, the increase of dynamic tension of the inclined mooring system can be more serious. When a long span is used instead, the elastic flexibility may help the situation.

For comparison, the dynamic behaviors of both types of SFTs against vertical ground motions are shown in Fig. 17. In vertical earthquakes, surge motions are almost negligible. Small heave motions occur in the M6.8 case. At any rate, the vertical-earthquake-induced SFT motions are very

small. Contrary to the horizontal-earthquake case, the pattern and rate of dynamic amplification for mooring tension of SFT-VM are similar to those of SFT-IM. In both cases, significant dynamic amplifications can be observed. At vertical earthquakes of M6.8, the maximum tension of SFT-VM is almost 25% larger than that of horizontal earthquakes.

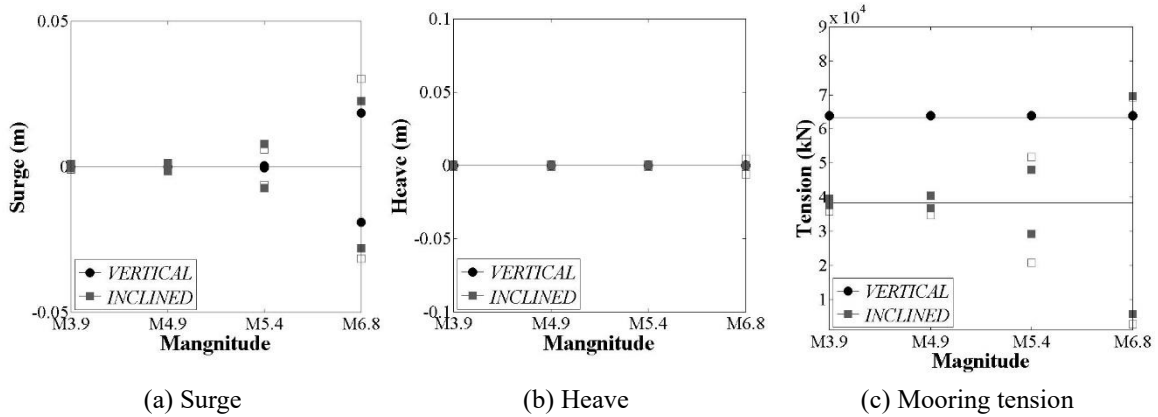


Fig. 14 Numerical results for (a) surge, (b) heave, and (c) tension (at fairlead) of vertical and inclined mooring lines under various real seismic horizontal motions (open marks represent OF and solid marks indicate CP.)

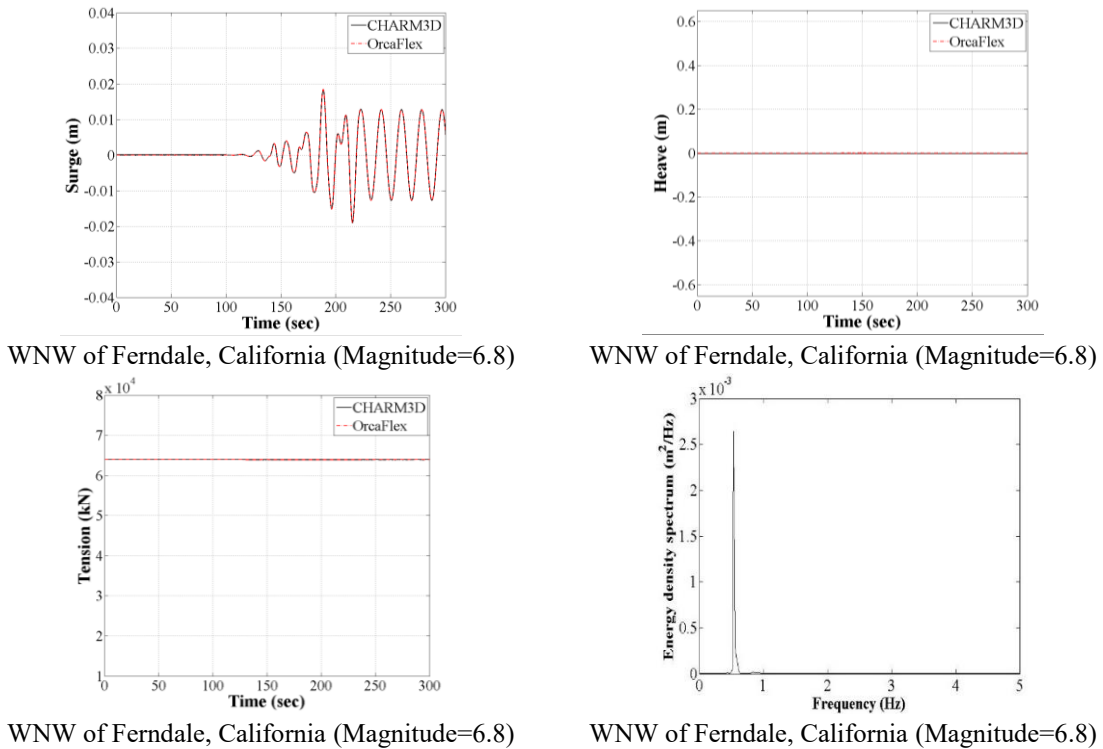


Fig. 15 Numerical results for (a) surge, (b) heave, (c) tension (at fairlead), and (d) surge spectrum of vertical mooring line with horizontal seismic excitations

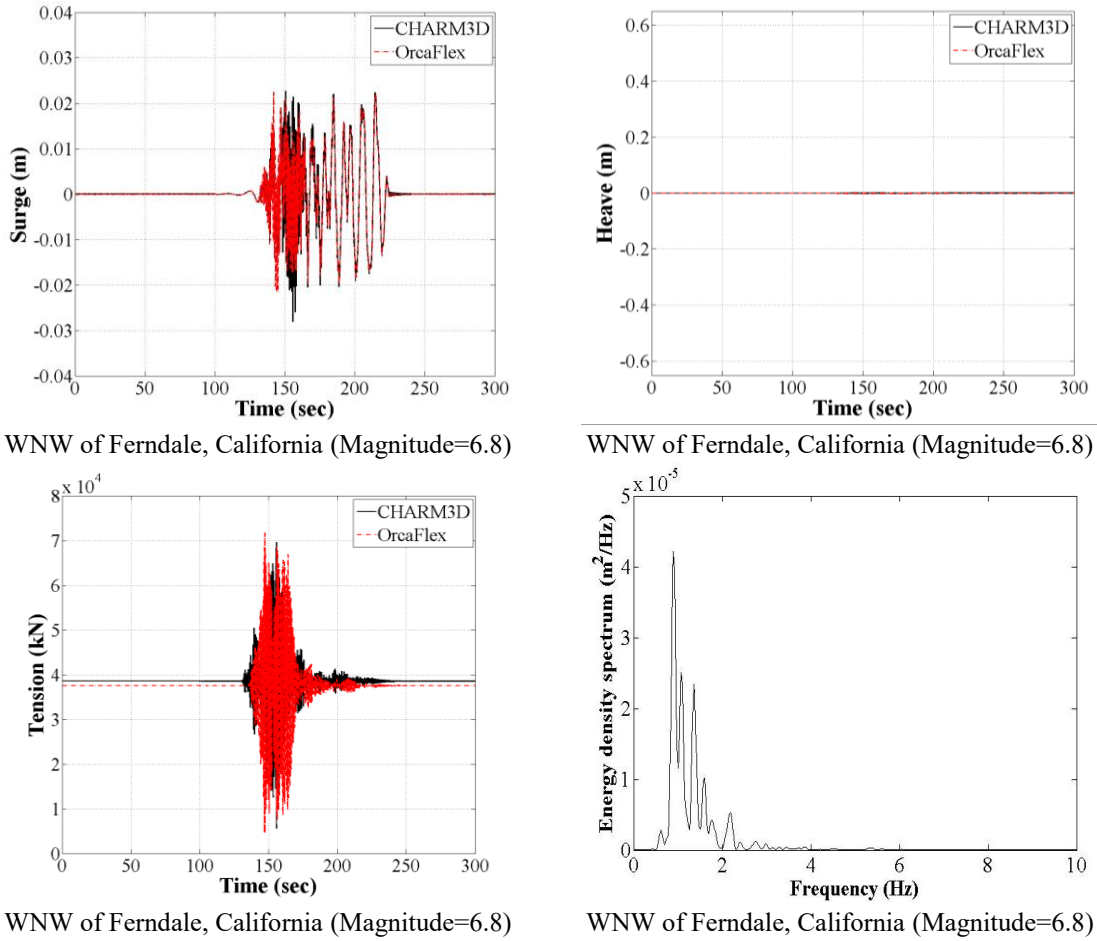


Fig. 16 Numerical results for (a) surge, (b) heave, (c) tension (at fairlead), and (d) surge spectrum of inclined mooring line with horizontal seismic excitations

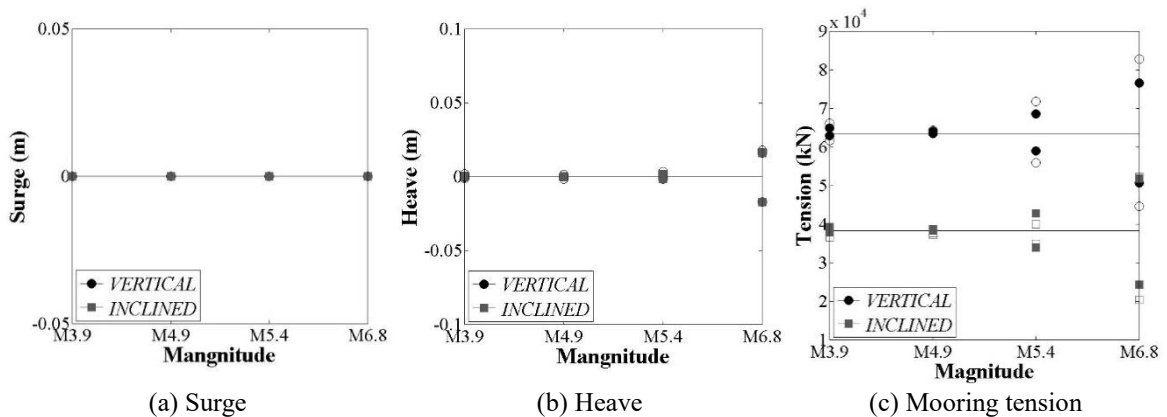


Fig. 17 Numerical results for (a) surge, (b) heave, and (c) tension (at fairlead) of vertical and inclined mooring lines under various vertical seismic excitations (open marks represent OF and solid marks denote CP.)

Finally, the horizontal and vertical ground motions of M6.8 are applied simultaneously, which is the closest to the actual case. The results are close to the superposition of those of horizontal and vertical earthquakes. It is seen that the maximum mooring tensions in this case are similar to the maximum tensions of either horizontal (SFT-IM) and vertical (SFT-VM) ground-motion cases.

5. Conclusions

The dynamic responses of two types of SFTs are analyzed for wave loads and/or seismic motions using numerical simulation tools, commercial program OF and in-house program CP. The dynamic motions and mooring tensions of a moored short-rigid SFT section with free ends are investigated. The effects of acoustic pressure induced by seismic motion due to fluid compressibility are not important for the global dynamics, so not included in the present study. The SFT numerical models were validated against Oh *et al.*'s (2013) model test results under regular wave conditions. Then the numerical models were further applied to the cases of irregular waves or seismic motions. The main results presented are SFT surge/heave motions and mooring tensions. The general trends and magnitudes obtained by the two different software packages reasonably agreed to each other along with experimental results.

SFTs are usually deeply submerged, so not affected by short waves or low to medium sea states. Under extreme wave conditions (high sea states), however, SFTs with free ends can move significantly with vertical mooring system both in surge and heave directions. Whereas, the inclined mooring system can very effectively restricts the SFT movement in such a harsh wave condition.

When seabed seismic motions are applied to the SFT system, the dynamic responses of SFTs are small but dynamic mooring tension can significantly be amplified. For example in M6.8 earthquake, the increase in dynamic tension is similar to that of extreme hurricane conditions. In particular for horizontal earthquakes, we see such a large tension increase in the inclined mooring system, while for vertical earthquakes, it happens for both inclined and vertical mooring systems. For smaller-scale earthquakes, the increase in tension is less significant. Especially when the earthquake frequencies are close to the natural frequencies of SFT motions and mooring dynamics, it can be even more dangerous, which has to be checked during the design procedure.

In the forthcoming study, the dynamic responses of long span SFTs with additional elastic flexibility are to be investigated. The effects of current including possible VIV (vortex induced vibration) are also to be investigated.

References

- Brancaleoni, F., Castellani, A. and D'asdia, P. (1989), "The response of submerged tunnels to their environment", *Eng. Struct.*, **11**(1), 47-56.
- Chen, W. and Huang, G. (2010), "Seismic wave passage effect on dynamic response of submerged floating tunnels", *Procedia Eng.*, **4**, 217-224.
- Chopra, Anil K. (2007), *Dynamics of Structures: Theory and Applications to Earthquake Engineering*, 4th Edition, Prentice Hall, New York, NY, USA.
- Cifuentes, C., Kim, S., Kim, M.H. and Park, W.S. (2015), "Numerical simulation of the coupled dynamic response of a submerged floating tunnel with mooring lines in regular waves", *Ocean Syst. Eng.*, **5**(2), 109-123.

- Dean, W.R. (1948), "On the reflection of surface waves by a submerged cylinder", *Math. Proc. Cambridge Philosoph. Soc.*, **44**(4), 483-491.
- DeCew, J., Tsukrov, I., Risso, A., Swift, M.R. and Celikkol, B. (2010), "Modeling of dynamic behavior of a single-point moored submersible fish cage under currents", *Aquac. Eng.*, **43**(2), 38-45.
- Di Pilato, M., Perotti, F. and Fogazzi, P. (2008), "3D dynamic response of submerged floating tunnels under seismic and hydrodynamic excitation", *Eng. Struct.*, **30**(1), 268-281.
- Fogazzi, P. and Perotti, F. (2000), "The dynamic response of seabed anchored floating tunnels under seismic excitation", *Earthq. Eng. Struct. Dyn.*, **29**(3), 273-295.
- Garrett, D.L. (1982), "Dynamic analysis of slender rods", *J. Energy Resour. Technol.*, **104**(4), 302-306.
- Hyun, C.H., Yun, C.B. and Lee, D.G. (1992), "Nonstationary response analysis of a suspension bridge for multiple support excitations", *Prob. Eng. Mech.*, **7**(1), 27-35.
- Kang, H.Y. and Kim, M.H. (2014), "Safety assessment of Caisson transport on a floating dock by frequency- and time-domain calculations", *Ocean Syst. Eng.*, **4**(2), 99-115.
- Lee, J.H. Seo, S.I. and Mun, H.S. (2016), "Seismic behaviors of a floating submerged tunnel with a rectangular cross-section", *Ocean Eng.*, **127**, 32-47.
- Long, X., Ge, F., Wang, L. and Hong, Y. (2009), "Effects of fundamental structure parameters on dynamic responses of submerged floating tunnel under hydrodynamic loads", *Acta Mechanica Sinica*, **25**(3), 335-344.
- Maruo, H. (1957), "The excess resistance of a ship in rough seas", *Int. Shipbuild. Prog.*, **4**(35), 337-345.
- Oh, S.H., Park, W.S., Jang, S.C., Kim, D.H. and Ahn, H.D. (2013), "Physical experiments on the hydrodynamic response of submerged floating tunnel against the wave action", *APAC*, 24-26.
- Orcina, (2015), *OrcaFlex Manual Version 9.8a*, Orcina, Ulverston, Cumbria, UK.
- Remseth, S., Leira, B.J., Okstad, K.M., Mathisen, K.M. and Haukas, T. (1999), "Dynamic response and fluid/structure interaction of submerged floating tunnels", *Comput. Struct.*, **72**(4), 659-685.
- Wheeler, J.D. (1969), "Methods for calculating forces produced by irregular waves", *Offshore Technology Conference*, 359-367.
- Yang, C.K. and Kim, M.H. (2010), "Linear and nonlinear approach of hydro-pneumatic tensioner modeling for spar global performance" *J. Offshore Mech. Arctic Eng.*, **132**(1), 011601.